Light scattering and nonlinear optical response near a critical point

Robert McGraw
Rockwell International Science Center, 1049 Camino Dos Rios, Thousand Oaks, California 91360
(Received 15 November 1989)

The connection between light scattering and nonlinear optical response is examined quantitatively for Kerr media and is generalized to include isotropic materials with nonlocal interactions near a critical point. A number of important quantities, including the nonlinear refractive index (n_2) and the four-wave-mixing coefficient, are shown to acquire increasing grating wave-vector ($\mathbf{q}$) dependence as the critical point is approached. This dependence is identical to the $\mathbf{q}$ dependence obtained for light scattering in the Ornstein-Zernike theory. Illustrative calculations are presented for near-critical xenon using the Redlich-Kwong equation of state and parameters obtained from independent measurements. These results indicate n_2 values of 10^{-15}–10^{-14} m^2/W and response times in the 1–10-μsec range. Calculations are presented for the phase-conjugate reflectivity in degenerate four-wave mixing that include both nonsaturable background loss and light-scattering noise. Reflectivities in excess of unity are predicted for 1.06-μm wavelength and cw pump intensities in the 10-kW/cm^2 range.

I. INTRODUCTION

For many classes of nonlinear optical materials the strength of the nonlinearity is proportional to the light-scattering efficiency of the medium. This connection has been demonstrated for artificial Kerr suspensions[1,2] as well as for more general Kerr media.[3,4] For quantum systems, it is exemplified by the well-known proportionality between the gain coefficient and the differential scattering cross section in the stimulated Raman effect.[5] Fluids near a critical point are known to be strong scatterers of light (critical opalescence), so such systems may be expected to be capable of high nonlinear activity as well. For example, in closely related systems, large nonlinearities have been measured in the isotropic phase of liquid crystals near a second-order isotropic-nematic phase transition that show the same temperature dependence [increasing as $(T-T^*)^{-1}$, where T^* is the transition temperature] as the increased light-scattering intensity in this region.[6] The following sections show that overall values for the Kerr coefficient, response time, and optical path length suggest that critical point fluids have exceptionally high potential for nonlinear optical signal processing applications. This is especially true for applications requiring low light absorption, strong nonlinear response over a wide frequency range, and tunable nonlinear response with small changes in either temperature or pressure of the medium. The present study was motivated in large part by experiments that are currently in progress to measure four-wave mixing and stimulated Rayleigh scattering in simple fluids such as Xe, SF_6, and freon near their respective critical points.[7]

The connection between ordinary light-scattering fluctuations and the nonlinear optical response properties of fluids is a fundamental one that has been examined in recent papers for systems outside of the critical region.[2–4] In addition to governing the nonlinear response, through the fluctuation-dissipation theorem, light-scattering fluctuations in the linear dielectric constant were also shown to determine the fundamental noise properties of the medium for nonlinear optical signal processing applications.[2–4] The objective of the present paper is to generalize these results through their extension to the near critical region. Here nonlocal interactions will be seen to have important consequences, both on the light scattering and on the nonlinear optical response.

For isotropic fluids, the change in dielectric constant induced by an applied electromagnetic field $\mathbf{E}$ is usually written as follows:

$$\epsilon(\mathbf{r})=\epsilon_0+\epsilon_2\mathbf{E}^2 , \tag{1.1}$$

where ϵ_0 is the background contribution and ϵ_2 determines the size of the nonlinear response. Clearly Eq. (1.1) applies only in the absence of long-range interactions, since it implies that the dielectric constant is a local function of the applied field. Application of the fluctuation-dissipation theorem to media for which the equilibrium dielectric response satisfies Eq. (1.1) gives[3,4]

$$\langle|\delta\epsilon(q)|^2\rangle=8\pi kT\epsilon_2/V_s , \tag{1.2}$$

where the angular brackets denote averaging over the beam interaction volume V_s. In deriving this result, the fluctuation component of $\epsilon(\mathbf{r})$ was resolved into its Fourier components with

$$\delta\epsilon(\mathbf{q})=(1/V_s)\int e^{i\mathbf{q}\cdot\mathbf{r}}\delta\epsilon(\mathbf{r})d^3\mathbf{r} , \tag{1.3}$$

where the region of integration is over the beam interaction volume. The quantity on the left side of Eq. (1.3) may be thought of as a fluctuation grating, which for a particular wave vector $\mathbf{q}$, namely that matching the wave vector of the laser-induced grating, will scatter light in the direction of the output field as noise. Note that the left side of Eq. (1.2) gives the mean-square amplitude for the change in dielectric constant due to thermal fluctua-

tions in the medium, while the right side gives the nonlinear optical response. Since ϵ_2 is a constant, both sides of Eq. (1.2) are seen to be independent of $\mathbf{q}$. This independence will be shown to break down when the range of interactions in the medium approaches the wavelength of light, resulting in a generalization of Eqs. (1.1) and (1.2) required for applications to the critical region. In the course of presenting these results, an independent derivation of Eq. (1.2) (appropriately generalized) based on thermodynamic fluctuation theory is obtained.

The symbols $\delta\epsilon(\mathbf{q})$ and $\Delta\epsilon(\mathbf{q})$ will be used throughout to designate the spontaneous fluctuation and field-induced gratings, respectively, each of wave vector $\mathbf{q}$. According to the Onsager regression hypothesis of irreversible thermodynamics,[8] it is impossible to determine *a priori* whether a given variation in the medium is the result of a spontaneous fluctuation, or due to the action of an applied field. For example, the light-scattering cross section will depend only on the amplitude and phase of the grating, and not on the manner by which it was formed. A typical scattering geometry is illustrated in Fig. 1(a). Here $\mathbf{K}_1$ and $\mathbf{K}_2$ are the wave vectors of the incident and scattered waves, respectively, θ is the scattering angle, and $\mathbf{q}$ is the wave vector of the grating. The same grating may be formed by writing beams having wave vectors $-\mathbf{K}_1$ and $-\mathbf{K}_2$, as shown in Fig. 1(b). Superimposition of Figs. 1(a) and 1(b) gives the standard four-wave-mixing configuration for nonlinear optical phase conjugation shown in Fig. 1(c).

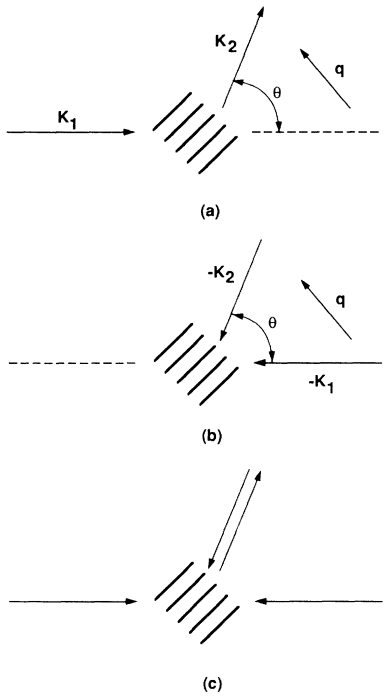

FIG. 1. Beam interaction geometry for (a) scattering of incident light of wave vector $\mathbf{K}_1$ to give scattered light of wave vector $\mathbf{K}_2$, (b) grating formation due to electrostriction in the presence of writing beams with wave vectors $-\mathbf{K}_1$ and $-\mathbf{K}_2$, and (c) superimposition of (a) and (b) showing typical configuration for optical phase conjugation via four-wave mixing. The grating wave vector $\mathbf{q}$ is equal to $\mathbf{K}_2-\mathbf{K}_1$.

The connection between light scattering and nonlinear optical response will be examined quantitatively and will be generalized to the near-critical region in Secs. II and III. There, the spontaneous fluctuations giving rise to light scattering will be shown to become increasingly wave-vector dependent as the critical point is approached. The simplest and most well-known model for this $\mathbf{q}$ dependence is provided by the Ornstein-Zernike (OZ) approximation[8,9] summarized in Sec. II. Corrections to the OZ approximation have been proposed, but these will not be used here since the uncorrected model has been found to be in good agreement with experiment over the temperature range of present interest.[9] Unfortunately, the OZ model does not describe the driven response of the medium to externally applied fields, which is necessary for the description of laser-induced gratings. Section III shows that the driven response is also modified in the critical region. In particular, the thermodynamic work required to produce a field-induced grating is found to acquire increasingly pronounced angular dissymmetry as the critical point is approached. Furthermore, the form of this new angular dependence is shown to correspond precisely to the $\mathbf{q}$ dependence obtained for the light-scattering fluctuations, so the fluctuation-dissipation relation is preserved. The generalization of Eqs. (1.1) and (1.2) to the near-critical region is also presented in this section, and the time response of medium is obtained. Illustrative calculations are carried out for xenon in Sec. IV using the Redlich-Kwong equation of state and parameters obtained from independent measurements. Calculations are presented for the phase-conjugate reflectivity in degenerate four-wave mixing (including scattering loss) and for the noise and response time characteristics of the medium. Section V concludes with a summary and discussion of results.

II. LIGHT SCATTERING IN THE ORNSTEIN-ZERNIKE APPROXIMATION

It is convenient to first obtain the density fluctuations in the medium ($\delta\rho(\mathbf{r})$). These can later be used to obtain $\delta\epsilon$ through the Clausius-Mossotti relation, or other similar approximation. Thus, the density-density correlation function is defined:

$$\mathbf{G}(\mathbf{r},\mathbf{r}')=\langle \delta\rho(\mathbf{r}),\delta\rho(\mathbf{r}')\rangle \ . \tag{2.1}$$

The scattered light intensity is proportional to the structure factor $S(\mathbf{q})$ where

$$S(\mathbf{q})=V_s^2\langle |\delta\rho(\mathbf{q})|^2\rangle \ . \tag{2.2}$$

Here the factor V_s^2 is used in conjunction with our volume-independent definition of the $\mathbf{q}$ transform given by Eq. (1.3). The structure factor and the density-density correlation function are related by Fourier transformation. For a uniform medium the dependence on $\mathbf{r}$ and $\mathbf{r}'$ is a function only of the relative position vector $R=\mathbf{r}-\mathbf{r}'$. Then the transform relation between Eqs. (2.1) and (2.2) is given as[8]

$$S(\mathbf{q})=V_s\int e^{i\mathbf{q}\cdot\mathbf{R}}G(\mathbf{R})d^3\mathbf{R} \ , \tag{2.3}$$

where, as in Eq. (1.3), the integration is over V_s.

To evaluate $S(\mathbf{q})$ using Eq. (2.3), standard practice is to rewrite the density-density correlation function in the form

$$G(\mathbf{R})=\langle\rho\rangle^2\Gamma(\mathbf{R})+\langle\rho\rangle\delta(\mathbf{R}) , \tag{2.4}$$

with

$$\Gamma(\mathbf{R})=g^{(2)}(\mathbf{R})-1 , \tag{2.5}$$

where $\langle\rho\rangle$ is the average density and $g^{(2)}$ is the pair distribution function. The delta function term in Eq. (2.4) gives the contribution from self-correlation. Remaining correlations are included in $\Gamma(\mathbf{R})$; for example, the product $\langle\rho\rangle^2 g^{(2)}(\mathbf{R})$ gives the density of particles at $\mathbf{R}$ given that a different particle is at the origin.

For media without interactions (ideal gases, liquid suspensions of noninteracting microparticles, etc.), the correlation function $\Gamma(\mathbf{R})=0$ and

$$G^0(\mathbf{R})=\langle\rho\rangle\delta(\mathbf{R}) , \tag{2.6}$$

where a superscript 0 is used to indicate the absence of interaction. Substitution into Eq. (2.3) gives

$$S^0(\mathbf{q})=\langle\rho\rangle V_s=\langle N\rangle , \tag{2.7}$$

where $\langle N\rangle$ is the average number of particles present in the beam interaction volume.

For simple fluids away from the critical point, interactions may be present but the interaction length, i.e., the range of G or Γ, is typically of order 10 Å, which is small compared with the wavelength of light. Under these conditions, the phase factor in Eq. (2.3) is slowly varying compared with $G(\mathbf{R})$ and may be replaced by unity. In this (small-$|\mathbf{q}|$) limit, Eq. (2.3) becomes independent of $\mathbf{q}$:

$$S(\mathbf{q})=V_s\int G(\mathbf{R})d^3\mathbf{R} . \tag{2.8}$$

The isothermal compressibility β_T can also be expressed in terms of the integral appearing in Eq. (2.8),[9]

$$\int G(\mathbf{R})d^3\mathbf{R}=\langle\rho\rangle^2 kT\beta_T , \tag{2.9}$$

a result that, like Eq. (1.2), is an expression of the fluctuation-dissipation theorem. Note that for Eq. (2.9) to be meaningful, the volume of integration V_s must include the full range of $G(\mathbf{R})$ in order that the compressibility be volume independent. Equations (2.2), (2.8), and (2.9) result in the well-known expression (due to Einstein) for the density fluctuations in a fluid:[8]

$$\langle|\delta\rho(\mathbf{q})|^2\rangle=\langle\rho\rangle^2 kT\beta_T/V_s . \tag{2.10}$$

The righthand side of this equation is explicitly independent of wave vector as a consequence of the small-$\mathbf{q}$ limit used to obtain Eq. (2.8).

Closer to the critical point of a fluid, the range of G becomes large and may approach or even exceed the wavelength of light. Where this occurs, the small-q assumption ($q=|\mathbf{q}|$) is violated and Eqs. (2.8) and (2.10), which are based on this assumption, need to be modified. A suitable modification may be obtained using the Ornstein-Zernike approach described more fully in Refs. 8 and 9. The final expression for the structure factor in the OZ approximation is given by Eq. (2.11) (see the Appendix),

$$S(\mathbf{q})/S^0(\mathbf{q})=\langle\rho\rangle kT\beta_T[1+(q/q_0)^2]^{-1} . \tag{2.11}$$

Substituting this result into Eq. (2.3) and carrying out the inversion gives

$$G(\mathbf{R})\rightarrow R_0^{-2}\exp(-q_0R)/R \tag{2.12}$$

as an asymptotic form for $G(\mathbf{R})$ at large R, where R_0 is the Debye persistence length (see the Appendix). The range of correlations is thus seen to be determined by $q_0^{-1}=\xi$, where ξ is the correlation length. In similar fashion, Eq. (2.10) for the density fluctuations is replaced by

$$\langle|\delta\rho(q)|^2\rangle=(\langle\rho\rangle^2 kT\beta_T/V_s)[1+(q/q_0)^2]^{-1} \tag{2.13}$$

as a consequence of Eqs. (2.2), (2.7), and (2.11).

In this section, the $\mathbf{q}$ grating was assumed to be the result of a fluctuation described by Eq. (2.13), as will be the case when no suitable applied fields are present. In Sec. III, the $\mathbf{q}$ grating will be examined as the response to writing beams such as those shown in Fig. 1(b). Since

$$q=2K\sin(\theta/2) , \tag{2.14}$$

where $K=|\mathbf{K}_1|=|\mathbf{K}_2|$, the square-bracketed expression in Eqs. (2.11) and (2.13) results in a *relative reduction* in density fluctuations for $q>0$ that give rise to scattering in all but the forward ($\theta=0$) direction. This reduction becomes important when the correlation length approaches distances of order q^{-1} [Eq. (2.13)]. Finally, we require for later use the intensity of light scattered per unit solid angle per unit volume per incident intensity I_0. This is given by the differential cross section, which is proportional to the structure factor through[8]

$$\sigma(\theta,\phi)=(\pi^2/\lambda^4)\left[\frac{\partial\epsilon}{\partial\rho}\right]^2(\sin^2\phi)S(\mathbf{q})/V_s . \tag{2.15}$$

Here λ is the vacuum wavelength of the incident light, ϕ is the angle between the wave vector of the scattered wave and the electric vector of the incident wave, and the pair of angles (θ,ϕ) defines the direction of scattering. Illustrative calculations of the stucture factor for near-critical xenon are presented in Sec. IV.

III. NONLINEAR RESPONSE

Next, we examine the case that the $\mathbf{q}$ grating is field induced. For this purpose, consider two degenerate plane-wave writing beams of frequency ω contributing to the total electric field $\mathbf{E}$:

$$\mathbf{E}=\mathbf{e}_1E_1\cos(-\mathbf{K}_1\cdot\mathbf{r}-\omega t)+\mathbf{e}_2E_2\cos(-\mathbf{K}_2\cdot\mathbf{r}-\omega t) , \tag{3.1}$$

where $\mathbf{e}_j$, E_j, and $-\mathbf{K}_j$ are the unit polarization vector, amplitude, and wave vector for wave j. [Note that the propagation wave vectors have been set equal to $-\mathbf{K}_1$ and $-\mathbf{K}_2$ to correspond to the writing beam configuration shown in Fig. 1(b).] The equilibrium elec-

trostrictive pressure equation is[10]

$$\nabla P - (8\pi)^{-1}\rho\frac{\partial\epsilon}{\partial\rho}\nabla\bar{\mathbf{E}}^2 , \tag{3.2}$$

where the overbar indicates averaging over an optical period. For the field specified by Eq. (3.1),

$$\bar{E}^2=(E_1^2+E_2^2)/2+(\mathbf{e}_1\cdot\mathbf{e}_2)E_1E_2\cos(\mathbf{q}\cdot\mathbf{r}) , \tag{3.3}$$

with $\mathbf{q}=\mathbf{K}_2-\mathbf{K}_1$. Equation (3.2) can now be used to obtain the medium response. However, in the presence of long-range correlations the following replacement, introduced by Fixman,[11,12]

$$\nabla P=\frac{\partial P}{\partial\rho}\text{grad}(\rho-q_0^{-2}\nabla^2\rho) , \tag{3.4}$$

must be used to obtain a valid equation in the density. The analysis used to derive Eq. (3.4) is somewhat involved and will not be repeated here since the details may be found in Ref. 12. The second term in parentheses becomes important when the correlation length approaches distances comparable to those over which the variation in density occurs. Substitution for the first term in Eq. (3.2) gives

$$\nabla\rho-q_0^{-2}\nabla^3\rho=(8\pi)^{-1}\rho^2\beta_T\frac{\partial\epsilon}{\partial\rho}\nabla\bar{\mathbf{E}}^2 , \tag{3.5}$$

where the relation

$$\beta_T=\rho^{-1}\frac{\partial\rho}{\partial P} \tag{3.6}$$

has been used. We now seek to determine the effect of Eq. (3.5) (particularly with its interaction term of order $q_0^{-2}\nabla^2\rho$) on the medium response.

Consider a general response to $\mathbf{E}$ of the form

$$\rho=\langle\rho\rangle+a_1\cos(\mathbf{q}\cdot\mathbf{r})+a_2\cos(2\mathbf{q}\cdot\mathbf{r})+\cdots \tag{3.7}$$

and denote by a_j^{eq}, the amplitude of the density grating of order j in equilibrium with the applied field. (For degenerate writing beam frequencies, there are no out-of-phase components to the medium response.) Keeping only the first-order grating term in the density and substituting into Eq. (3.5) gives

$$a_1^{\text{eq}}=[1+(q/q_0)^2]^{-1}(8\pi)^{-1}\langle\rho\rangle^2\beta_T\frac{\partial\epsilon}{\partial\rho}(\mathbf{e}_1\cdot\mathbf{e}_2)E_1E_2 , \tag{3.8}$$

where Eq. (3.3) has been used. Comparison of Eqs. (2.13) and (3.8) shows that an important effect of the long-range correlations near the critical point is to reduce the field-induced grating response by precisely the same factor that these correlations reduce the spontaneous fluctuations of the same wave vector $\mathbf{q}$. Thus, identical angular dissymmetry is obtained for both the light-scattering fluctuations and the first-order (but still nonlinear in field strength on account of the product E_1E_2) response.

A. Free energy of grating formation

The underlying reason for the reduction in grating response seen in Eq. (3.8) may be qualitatively explained as follows. As the range of correlations approaches the spatial period of a field-induced grating, it takes more work to make the grating. This extra work is needed to break correlations that would otherwise be present if the medium were uniform. The same reasoning applies to the reduction of spontaneous fluctuations [Eq. (2.13)] as well. A quantitative analysis of the free energy of grating formation must include contributions from field-induced polarization as well as the work required to create the nonuniformity in the medium that comprises the grating itself. The free energy of nonuniformity was obtained by Debye[13] and by Fixman,[12] who showed equivalence between the Debye and Ornstein-Zernike approaches, upon observing that the correction for nonlocality in Eq. (3.4) is equivalent to the addition of a squared gradient term to the free-energy density to give[12]

$$F_i=\tfrac{1}{2}\rho\frac{\partial P}{\partial\rho}(s^2+q_0^{-2}|\nabla s|^2) . \tag{3.9}$$

Here $s=(\rho-\langle\rho\rangle)/\langle\rho\rangle$ is the fractional change in density and the term in s^2 gives the free energy of inhomogeneity in the absence of long-range interactions. Substituting from Eq. (3.7) and averaging over volume gives

$$\langle F_i\rangle=\tfrac{1}{4}(\rho^2\beta_T)^{-1}\{a_1^2[1+(q/q_0)^2]+a_2^2[1+(2q/q_0)^2]+\cdots\} \tag{3.10}$$

for this contribution to the change in free-energy density. As expected from the previous discussion, more work is required in the Fixman model to create the shorter spaced higher-order gratings. [Equation (3.10) is valid only when the grating amplitudes are small, otherwise the full nonlinear behavior contained in Eq. (3.5) needs to be included. The validity of this assumption is confirmed via numerical solution of Eq. (3.5) for near-critical xenon in Sec. IV.] Note that for media without interactions, Eq. (3.10) has a simple interpretation in that it gives the work required to achieve configurational entropy reduction in conjunction with the formation of an ordered grating.

The second contribution to the free-energy density arises from the coupling of the applied field to the nonlinear polarization of the medium and is of the form[10]

$$F_e=-\tfrac{1}{2}\mathbf{P}_{\text{NL}}\cdot\mathbf{E} , \tag{3.11}$$

where $\mathbf{P}_{\text{NL}}=(\Delta\epsilon/4\pi)\mathbf{E}$ is the nonlinear polarization. With $\Delta\epsilon=(\partial\epsilon/\partial\rho)\Delta\rho$, Eq. (3.11) becomes

$$\langle F_e\rangle=-(16\pi)^{-1}\frac{\partial\epsilon}{\partial\rho}(\mathbf{e}_1\cdot\mathbf{e}_2)E_1E_2a_1 \tag{3.12}$$

plus a constant contribution due to the rectification terms in Eq. (3.3), which we may set equal to zero with a suitable choice of energy scale. [Consistency with Eq. (3.10) then requires that $\langle\rho\rangle$ be defined as the average density in the illuminated region, and not as the average over the entire sample volume, which may differ due to electrostriction.]

Adding Eqs. (3.12) and (3.10) gives an expression for the total free-energy density $\langle F\rangle=\langle F_i\rangle+\langle F_e\rangle$ as a quadratic function of the grating coefficients $\{a_1,a_2,\ldots\}$

in the form

$$\langle F\rangle = Aa_1^2 - Ba_1 + \cdots , \tag{3.13}$$

where the coefficients A and B are defined through Eqs. (3.10) and (3.12), respectively, and the unwritten terms refer to the contribution from higher-order gratings. The minimum in this multidimensional free-energy surface occurs at $a_1 = a_1^{eq}$, $a_2 = 0$, etc., where the equilibrium grating amplitude $a_1^{eq} = B/2A$ is identical to the result previously given by Eq. (3.8).

Fluctuations in the grating coefficients may be obtained from the curvature of the free-energy surface near its minimum value. From standard thermodynamic fluctuation theory, the probability of a given set of coordinates $\{a_1, a_2, \ldots\}$ occurring spontaneously is proportional to

$$\exp(-W\{a_1, a_2, \ldots\}/kT) ,$$

where

$$W\{a_1, a_2, \ldots\} = V_s\langle F\rangle$$

is the reversible work required to create the configuration under the application of constraints. Inspection of Eqs. (3.10)–(3.13) shows that the fluctuations in each coordinate are independent and Gaussian in form with

$$\langle|\delta a_1|^2\rangle = 2(\langle\rho\rangle^2 kT\beta_T/V_s)[1+(q/q_0)^2]^{-1} . \tag{3.14}$$

This result is in agreement with Eq. (2.13) after including a factor of $\frac{1}{2}$ for the average over V_s of $\cos^2$ for the fluctuations in density. Note that to this order of approximation the mean-square grating fluctuation amplitude, being independent of the B term in Eq. (3.13), is independent of the applied field. This will not be the case when the field strength is sufficiently strong that saturation effects prevail. However, for simple critical-point fluids, the saturation field strengths are much higher than those likely to be usefully achieved (Sec. IV). Fluctuations in a_j also follow Eq. (3.14), except that q is replaced by $j\times q$ in the square-bracketed correction for long-ranged interaction.

B. Dielectric response in the presence of nonlocal interaction

A nonlocal generalization of Eq. (1.1) may be written in terms of the convolution integral:

$$\epsilon(\mathbf{r}) = \epsilon_0 + \int \epsilon_2(\mathbf{r}-\mathbf{r}')\mathbf{E}^2(\mathbf{r}')d^3\mathbf{r}' , \tag{3.15}$$

for an isotropic medium. Fourier transformation [cf., Eq. (1.3)] gives

$$\epsilon(\mathbf{q}) = \epsilon_0\delta(\mathbf{q}) + \epsilon_2(\mathbf{q})\mathbf{E}^2(\mathbf{q}) . \tag{3.16}$$

Now since

$$\epsilon(\mathbf{q}) = \frac{\partial\epsilon}{\partial\rho}a_1^{eq}/2 = \epsilon(-\mathbf{q})$$

and

$$\mathbf{E}^2(\mathbf{q}) = \mathbf{e}_1\cdot\mathbf{e}_2 E_1 E_2/2$$

from Eqs. (3.7) and (3.3), respectively, we obtain

$$\epsilon_2(\mathbf{q}) = (8\pi)^{-1}\langle\rho\rangle^2\beta_T\left[\frac{\partial\epsilon}{\partial\rho}\right]^2[1+(q/q_0)^2]^{-1} . \tag{3.17}$$

for the nonlinear dielectric constant, and

$$\langle|\delta\epsilon(\mathbf{q})|^2\rangle = \langle|\delta\rho(\mathbf{q})|^2\rangle\left[\frac{\partial\epsilon}{\partial\rho}\right]^2 = (\langle\rho\rangle^2 kT\beta_T/V_s)[1+(q/q_0)^2]^{-1}\left[\frac{\partial\epsilon}{\partial\rho}\right]^2 \tag{3.18}$$

for the mean-square fluctuation amplitude using Eq. (2.13). Comparison of Eqs. (3.17) and (3.18) provides the independent derivation and generalization of Eq. (1.2) that we have been seeking:

$$\langle|\delta\epsilon(\mathbf{q})|^2\rangle = 8\pi kT\epsilon_2(\mathbf{q})/V_s . \tag{3.19}$$

Apart from its $\mathbf{q}$ dependence, this expression is identical in form to our previous result and supports the validity of the fluctuation-dissipation approach, previously used to derive Eq. (1.2),[3] even in the presence of nonlocal interactions. Equation (3.19) will be used in Sec. IV to predict the light-scattering noise inherent in a phase-conjugate signal obtained by degenerate four-wave mixing.

It is useful to explore the generality of Eq. (3.19), since here its derivation was obtained specifically using (1) the OZ correction for light scattering, and (2) the Fixman square-gradient modification to obtain the free-energy component due to inhomogeneity in the medium response. That Eq. (3.19) is more general may be seen as follows: First, note that (1) and (2) are mutually consistent; indeed they are equivalent, through thermodynamic fluctuation theory. To see this, recall that Eq. (3.10) (which results from the Fixman correction) provides the A coefficient appearing in Eq. (3.13). This coefficient alone determines the curvature of the free-energy surface, thereby fixing the mean-square amplitude of the Gaussian fluctuations in the dielectric constant. If these fluctuations are to satisfy the Ornstein-Zernike relation, then it is clear that the A coefficient, and hence the Fixman correction itself, are uniquely determined. Second, the A coefficient, and therefore *any* modification of the light scattering, cancels in deriving Eq. (3.19). Thus the generalization of this result, beyond any specific form imposed on the scattering by the OZ correction, is established. One may, for example, obtain the dielectric fluctuations directly from low-intensity scattering experiments and then use Eq. (3.19) to predict the nonlinear optical response as well as the light-scattering noise characteristics of the medium.

C. Time response

Comparison of critical-point fluids with other classes of nonlinear materials for real-time signal processing applications requires an examination of their time response. This may be defined as the characteristic time required for relaxation of a grating once the writing beams used to form that grating have either been switched off or changed so that a new grating can be formed. Note that

the time required to form the grating is either the same as the decay time, for weak fields, or shorter, for field strengths in the driven regime. In either case, the rate determining step is the time required for the grating to decay, which is conveniently obtained from the frequency dependence of the fluctuation spectrum $S(q,\Omega)$.

The fluctuations represented in

$$S(q)=(2\pi)^{-1}\int S(q,\Omega)d\Omega$$

include both the central Rayleigh (entropy fluctuations at constant pressure) and Brillouin (pressure fluctuations at constant entropy) components of the spectrum.[14] From Landau-Placzek theory, it is known that as T approaches T_c the Rayleigh component increases sharply and, in the limit, equals the total intensity, while the integrated intensity of the Brillouin doublet varies smoothly near the critical point.[14] Consequently, the sharp increase in nonlinear optical properties predicted for the critical region results from the enhancement of the Rayleigh fluctuations (i.e., enhancement of stimulated Rayleigh scattering) and is not due to enhancement of stimulated Brillouin scattering (SBS). This last result suggests that the medium response time may be obtained directly from measurements of the Rayleigh linewidth in the critical region.

The Rayleigh linewidth has been measured for a number of fluids near the critical point and has been shown to follow the well-known Kawasaki mode-coupling form

$$\Gamma=(kT/8\pi\eta\xi^3)\times\{1+(q\xi)^2+[(q\xi)^3-(q\xi)^{-1}]\arctan(q\xi)\}\ , \qquad (3.20)$$

where η is the high-frequency part of the shear viscosity. This expression has been successfully applied to the interpretation of linewidth measurements for near-critical xenon in Ref. 15. In the hydrodynamic limit ($q\xi \ll 1$), Eq. (3.20) reduces to the Landau-Placzek result $\Gamma=(kT/6\pi\eta\xi)q^2$. Since η has no critical anomaly, the response time $\tau=1/\Gamma$ is seen to increase as ξ in the hydrodynamic regime. In the limit very close to the critical point ($q\xi \gg 1$), Eq. (3.20) approaches $\Gamma=(kT/16\eta)q^3$ showing that the linewidth and response time become independent of reduced temperature. For the intermediate, or Fixman-Botch regime ($q\xi\approx 1$), it was first suggested that the inclusion of the nonlocal pressure term results in a correction to the hydrodynamic Rayleigh linewidth of the form

$$\Gamma=(kT/6\pi\eta\xi)q^2[1+b(q\xi)^2]$$

with $b=1$. Inspection of the mode-coupling result [Eq. (3.20)] shows that this form is correct but that $b=\frac{3}{5}$ rather than unity in this regime.[15]

IV. ILLUSTRATIVE CALCULATIONS WITH APPLICATIONS TO DEGENERATE FOUR-WAVE MIXING

The foregoing theory is used in this section to predict the light-scattering, nonlinear optical response, and noise properties of a representative critical-point medium. General solutions are given for four-wave mixing, which include for the first time both scattering loss and noise. Where specific parameters are required to illustrate the size of the effects described, those corresponding to xenon are used. Nevertheless, other isotropic fluids will be expected to show similar behavior when results are expressed in a suitable scaling form.

A. Parameters for xenon

Calculations of the nonlinear optical response were carried out for xenon as a model critical-point fluid using the Redlich-Kwong equation of state:

$$P=[RT/(V-\beta)]-\alpha T^{-1/2}/[V(V+\beta)]\ , \qquad (4.1)$$

with parameters $\alpha=6.220\,14$ and $\beta=30.7459\times10^{-6}$ in mks units. These parameters were determined to give a critical point at $T_c=289.73$ K and density $\rho_c=8453.9$ mol/m^3 in agreement with experiment.[16] Figure 2 shows the isothermal compressibility (m^3/J) obtained from Eqs. (3.6) and (4.1) for $T-T_c=1.0$, 0.25, and 0.10 K as a function of density in the critical region. At a constant density, equal to ρ_c, the best-fit expression

$$\beta_T=1.7604\times10^{-8}T_r^{-1.000}\ , \qquad (4.2)$$

where $T_r=(T-T_c)/T_c$ is the reduced temperature, provides an excellent representation of the isothermal compressibility calculated over the temperature range of interest from the equation of state. [Equation (4.2) yields an incorrect value for the critical exponent, as may be expected from a modified van der Waals equation of state. Instead of -1, the measured value for the compressibility exponent has been reported as -1.241,[16] but this difference is not expected to have a significant bearing on the present results, or on their implications for nonlinear optics applications.] The quantity q_0 is obtained from the correlation length using $\xi=\xi_0 T_r^{-0.63}$, with $\xi_0=2.0\times10^{-10}$ m from Ref. 16. The Clausius-Mossotti

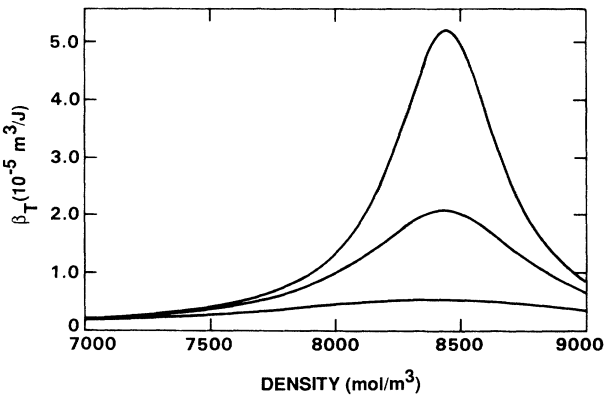

FIG. 2. Isothermal compressibility of xenon calculated using the Redlich-Kwong equation of state for $T-T_c=1.0$ K (lower curve), 0.25 K (middle curve), and 0.1 K (upper curve).

constant $\partial\epsilon/\partial\rho$ appearing in Eq. (3.5) was obtained using the relation

$$\frac{\partial\epsilon}{\partial\rho}=(\epsilon-1)(\epsilon+2)/3\rho \ ,$$

with $\rho=\rho_c$ and $\epsilon_0=1.295$ from the measured refractive index,[17] to give $\partial\epsilon/\partial\rho=3.833\times10^{-5}$.

B. Light scattering and nonlinear response

The fundamental connection between the light scattering and nonlinearity, seen here to be preserved for systems with long-ranged interactions, is illustrated for xenon at two different wavelengths in Figs. 3 and 4. In particular, this connection enables both the four-wave-mixing coefficient (left-hand scale) and the structure factor (right-hand scale) to be represented by the same family of curves corresponding top to bottom (in the cluster of four curves) to angles $\theta=0°$, 45°, 90°, and 180° in Eq. (2.14). Here the four-wave-mixing coefficient is

$$\kappa_0(\mathbf{q})=\epsilon_2(\mathbf{q})QE_0^2/2\epsilon_0 \ , \tag{4.3}$$

where we have assumed equal amplitudes E_0 for the counterpropagating pump beams (the pump intensities were set at 10 kW/cm^2 in the present calculation of κ_0) and ϵ_2 is given by Eq. (3.17). From Eq. (4.3), it follows that, near the critical temperature, κ_0 is also dependent on $\mathbf{q}$. The structure factor ratio is given by Eq. (2.11). Figure 3 shows the relative reduction in both the structure factor and four-wave-mixing coefficient for $\theta=180°$ (relative to the $\theta=0°$ case) by about 35% at $T-T_c=0.1$ K ($T_r=3.45\times10^{-4}$) for $\lambda=5145$ Å. The former implies an equivalent reduction in back-scattered light intensity [see Eq. (2.15)] predicted by the OZ theory. In addition, the figure shows approximately 1000-fold increase in structure factor overall, relative to S^0, due to the proximity of the critical point. This increase is ultimately responsible for the enhanced nonlinear optical properties predicted for critical-point fluids, as well as for the increased light scattering observed in the critical region.

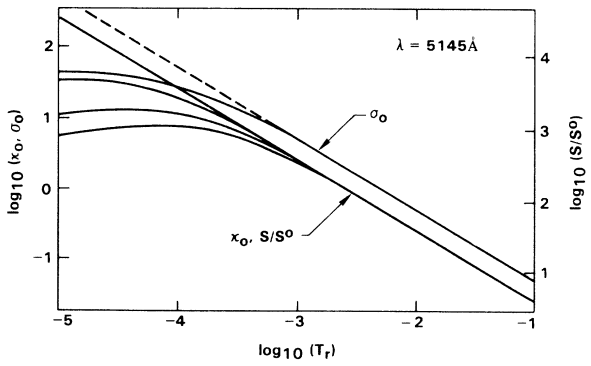

FIG. 3. Four-wave-mixing coefficient (m^{-1}), structure factor, and scattering attenuation coefficient for xenon. Curves for κ_0 and S are, top to bottom, for $\theta=0°$, 45°, 90°, and 180°. Curves for σ_0 are from Eq. (4.4) for isotropic scattering (dashed), and Eq. (4.5), which includes the Ornstein-Zernike correction (solid). Results were obtained for $\lambda=5145$ Å.

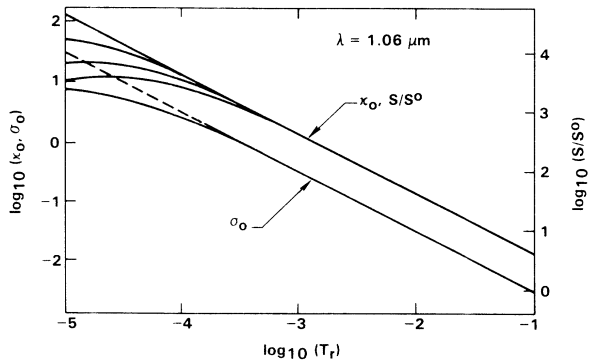

FIG. 4. Same as for Fig. 3 but for $\lambda=1.06$ μm.

The upper pair of curves in Fig. 3 (lower pair in Fig. 4) compares the calculated scattering attenuation coefficient, as a function of T_r, with and without the $\mathbf{q}$ dependence described by the OZ theory included. The dashed line gives the usual light-scattering attenuation coefficient σ_0 for isotropic scattering:

$$\sigma_0=8\pi^3\beta_T\left[\rho\left[\frac{\partial\rho}{\partial\epsilon}\right]\right]^2 kT\Big/(3\lambda^4\epsilon_0^2) \ , \tag{4.4}$$

This expression neglects the angular dissymmetry of scattering described in Sec. II and is expected, therefore, to be valid only sufficiently far from the critical point. To include the OZ corrections, σ_0 was obtained by numerical integration of the differential scattering cross section given by Eq. (2.15):

$$\sigma_0=\int\int\sigma(\theta,\phi)\sin\phi\, d\theta\, d\phi \tag{4.5}$$

over all scattering angles $0\le\theta\le2\pi$, $0\le\phi\le\pi$. The angular dependence of the integrand follows from Eqs. (2.11), (2.14), and (2.15). Integration was performed using a Monte Carlo technique consisting of random sampling and averaging over a sufficient number of scattering angles that, for specific T_r and wavelength, convergence was obtained. The results of these calculations are shown by the appropriately labeled solid curves in Figs. 3 and 4. Near the critical point the suppression of light-scattering fluctuations is seen to result in a reduction in the scattering attenuation coefficient relative to the predicted isotropic scattering result [Eq. (4.4)]. Also confirmed is that Eqs. (4.4) and (4.5) yield equivalent results at temperatures outside the critical region.

In the derivation of Eqs. (3.10) and (3.14), the medium was assumed to be far from saturation so that the grating amplitudes were small. To confirm this assumption, Eq. (3.5) was solved numerically by self-consistent iteration until convergence was obtained. Each iteration step used a Runge-Kutta integration with β_T computed as a function of density, at fixed temperature, directly from the equation of state. Once the converged solution was obtained (after only a few iterations), it was Fourier decomposed into its various grating orders for examination. Typically, for example with xenon at $T-T_c=0.1$ K and writing beam intensities of 10 kW/cm^2, the numerical solution gives for $\langle\rho\rangle=\rho_c=8453.9$, $a_1^{eq}=2.8\times10^{-2}$, and

TABLE I. Grating response time and nonlinear refractive index for xenon. Response times are equal to the reciprocal of the measured Rayleigh linewidth from Ref. 15. See text for calculation of n_2.

	$\lambda=5145$ Å		$\lambda=1.06$ μm	
$\text{Log}_{10}(T_r)$	τ (μsec)	n_2 (10^{-15} m^2/W)	τ (μsec)	n_2 (10^{-15} m^2/W)
−5.0	14.4	5.75	125.0	22.9
−4.5	14.2	7.27	116.0	24.3
−4.0	12.8	7.73	82.0	17.3
−3.5	8.55	5.48	41.5	7.73
−3.0	4.20	2.45	18.2	2.71
−2.5	1.81	0.86	7.72	0.88
−2.0	0.77	0.28	3.26	0.28

$a_2^{eq}=1.5\times10^{-7}$ for use in Eq. (3.7). The density variation in the first-order grating is thus seen to be less than one part in 3×10^5, clearly showing that the medium is far from saturation and that the grating amplitudes are small. As further confirmation that the perturbative approach to Eq. (3.5) is valid, we note that the value of a_1^{eq} obtained analytically from Eqs. (3.8) and (4.2) coincides with the above numerical value.

Response times for xenon were obtained from a fit of the measured Rayleigh linewidth data to the mode-coupling form [Eq. (3.20)] reported in Ref. 15. The results are listed here for the two wavelengths $\lambda=5145$ Å and $\lambda=1.06$ μm as functions of reduced temperature in Table I. For each wavelength, the grating q value was calculated from Eq. (2.14) setting θ equal to 180°. The linewidth dependencies on q and T_r, discussed in connection with Eq. (3.20), are reflected in the tabulated time response. Corresponding values of the nonlinear index

$$n_2(\mathbf{q})=\epsilon_2(\mathbf{q})/2n_0$$

are also tabulated with $\epsilon_2(\mathbf{q})$ obtained from Eq. (3.17). Here the dominant effect of long-range correlations is that n_2 does not diverge with the isothermal compressibility, but instead appears to be bounded as the critical temperature is approached. The dependence of n_2 on $\mathbf{q}$ (seen here as a dependence on wavelength) is also seen to be reduced with increasing distance from the critical point.

While long-range correlations in the medium are seen here to lower n_2, they are also seen to result in an increase in the scattering length in a manner that is favorable to achieving a long beam interaction length for nonlinear wave mixing. In addition, a favorable leveling off of the medium response time is found as the critical point is approached.

C. Four-wave mixing with nonsaturable background loss and light-scattering noise

The present treatment follows closely that of Pepper and Yariv for phase conjugation in Kerr-like media having nonsaturable background loss,[18] but also includes light-scattering noise. (Our previous treatment of light-scattering noise in four-wave mixing, presented in Ref. 4, was limited to noncritical media and neglected the effects due to nonsaturable background loss.) As in Ref. 18, both the probe and conjugate waves are considered to be weak to the extent that stimulated scattering contributions to phase conjugation may be neglected. The wave equation for the nonlinear medium,with the noise fluctuations $\delta\epsilon$ included, is[4]

$$\nabla^2\mathbf{E}(\mathbf{r},t)=-(\omega^2/c^2)(\epsilon_0+\epsilon_2\bar{\mathbf{E}}^2+\delta\epsilon)\mathbf{E}(\mathbf{r},t)\ , \tag{4.6}$$

where $\mathbf{E}(\mathbf{r},t)$ is the total field. Note that any q dependence suppressed in this section for notational simplicity is to be understood. For degenerate four-wave mixing,

$$\mathbf{E}(\mathbf{r},t)=\tfrac{1}{2}(\mathbf{e}_pE_pe^{i\mathbf{Q}\cdot\mathbf{r}}+\mathbf{e}_cE_ce^{-i\mathbf{Q}\cdot\mathbf{r}}+\mathbf{e}_1E_0e^{i\mathbf{K}\cdot\mathbf{r}}+\mathbf{e}_2E_0e^{-i\mathbf{K}\cdot\mathbf{r}}+\text{c.c})e^{-i\omega t}\ , \tag{4.7}$$

where we assume equal pump amplitudes $E_1=E_2=E_0$ and E_p (E_c) is the slowly varying envelope of the probe (conjugate) wave. Here we have departed from the notation of Fig. 1 in that $\pm\mathbf{K}$ are the wave vectors of the counterpropagating pump beams, and $\mathbf{Q}$ ($-\mathbf{Q}$) is the wave vector of the probe (conjugate) wave. Substitution of Eq. (4.7) into Eq. (4.6) gives, for the collinear field geometry of Fig. 5,[4,18]

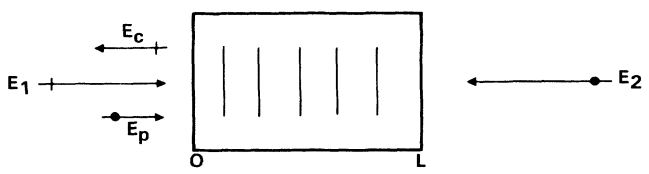

FIG. 5. Four-wave-mixing geometry. The symbols ● and | indicate vertical and horizontal beam polarization, respectively. Writing beams are E_p and E_2 with $\theta=180°$. Note that the beam polarizations were chosen so that only a single grating is formed.

$$\frac{dE_c}{dz} = -i\kappa_0 \exp(-\alpha_0 L/2)(E_p^*/2 + E_c) + (\alpha_0/2)E_c - i\mathcal{L}(z) , \tag{4.8a}$$

$$\frac{dE_p^*}{dz} = -i\kappa_0 \exp(-\alpha_0 L/2)(E_p^* + E_c/2) - (\alpha_0/2)E_p^* - i\mathcal{L}(L-z) . \tag{4.8b}$$

Here L is the beam interaction length, α_0 is the attenuation coefficient for nonsaturable background loss, and the slowly varying envelope and phase approximation has been used. Note that for the beam polarizations shown in Fig. 5, only a single (180°) grating is formed. This accounts for the additional factor of $\frac{1}{2}$ preceding E_p^* and E_c in Eqs. (4.8a) and (4.8b). The noise operator $\mathcal{L}$ is defined as[4]

$$\mathcal{L}(z) = QE_0(z)\delta\epsilon/2\epsilon_0 = QE_0 \exp(-\alpha_0 z/2)\delta\epsilon/2\epsilon_0 = \gamma \exp(-\alpha_0 z/2) , \tag{4.9}$$

where the last equality defines the complex z-independent noise variable γ.

To obtain the solution to Eqs. (4.8) and (4.9), it is convenient to introduce a few variable transformations. First, let

$$\kappa_1 = (\kappa_0/2)\exp(-\alpha_0 L/2) \tag{4.10}$$

and

$$\kappa_{\text{eff}} = [\kappa_1^2 - (\alpha_0/2)^2]^{1/2} . \tag{4.11}$$

Following Ref. 18, we next introduce the variables

$$A(z) = E_p^*(z)\exp(2i\kappa_1 z + \alpha_0 z/2)$$

and

$$B(z) = E_c(z)\exp[2i\kappa_1 z - \alpha_0(z-L)/2] .$$

Equations (4.8) may then be written in the form

$$\frac{dB}{dz} = -i\kappa_1 A \exp[-\alpha_0(z - L/2)] - i\gamma \exp(2i\kappa_1 z)\exp[-\alpha_0(z - L/2)] , \tag{4.12a}$$

$$\frac{dA}{dz} = -i\kappa_1 B \exp[\alpha_0(z - L/2)] - i\gamma \exp(2i\kappa_1 z)\exp[\alpha_0(z - L/2)] . \tag{4.12b}$$

We now require the solution to Eqs. (4.12) and (4.9) subject to the usual boundary conditions (cf., Fig. 5): $E_c(L) = B(L) = 0$ and $A(0) = E_p^*(0)$. This is readily obtained for constant γ and, in particular, for $\gamma = 0$ gives the standard result for four-wave mixing in a lossy medium in the absence of noise.[18] For nonzero γ, we obtain

$$B(z) = c_1 \exp(-\alpha_0 z/2)\sin(\kappa_{\text{eff}} z) + c_2 \exp(-\alpha_0 z/2)\cos(\kappa_{\text{eff}} z) + y_p(z) , \tag{4.13}$$

where $y_p(z)$ is a particular solution of the second-order differential obtained by eliminating $A(z)$ from Eqs. (4.12):

$$y_p(z) = -[2\gamma/(3\kappa_1 + 2i\alpha_0)]\exp(2i\kappa_1 z) \times \exp[-\alpha_0(z - L/2)] + [\gamma/(3\kappa_1 - 2i\alpha_0)]\exp(2i\kappa_1 z) . \tag{4.14}$$

The coefficients c_1 and c_2 are obtained from Eqs. (4.12a) and (4.13) using the boundary conditions specified above. [The solution for $A(z)$ is of the same form except that α_0 is replaced with $-\alpha_0$ in Eqs. (4.13) and (4.14).] Upon converting back to original notation, the solutions are

$$E_c(0) = B(0)\exp(-\alpha_0 L/2)$$

and

$$E_p^*(L) = A(L)\exp(-2i\kappa_1 L - \alpha_0 L/2) ,$$

respectively, for the phase-conjugate and transmitted probe fields.

Figures 6–8 show the predicted phase-conjugate reflectivity for xenon, defined by the intensity ratio

$$R = [E_c(0)E_c^*(0)]/[E_p^*(0)E_p(0)] , \tag{4.15}$$

as computed from Eqs. (4.13) and (4.14) in the absence of noise ($\gamma = 0$). Since the only significant loss mechanism for xenon is light scattering itself, the attenuation coefficient α_0 was set equal to σ_0 in the calculations, with the latter determined from Eq. (4.5). Figures 6 and 7 differ only in wavelength and were derived assuming cw pump intensities of 10 kW/cm^2. The most significant difference lies in the size of the maximum reflectivities obtained. For $\lambda = 5145$ Å, the maximum reflectivity is about one percent at this pump intensity while for $\lambda = 1.06$ μm reflectivities in excess of unity are obtained. This sensitivity to wavelength is also manifested in the relative positioning of the curves for κ_0 and σ_0 in Figs. 4 and 5. At $\lambda = 1.06$ μm, κ_0 exceeds σ_0 to the extent that, even with losses included, κ_{eff} [Eq. (4.11)] takes on real values. This last condition, not satisfied at $\lambda = 5145$ Å, is necessary for R to exceed unity. Indeed, if the pump power is increased only slightly above 10 kW/cm^2 at the

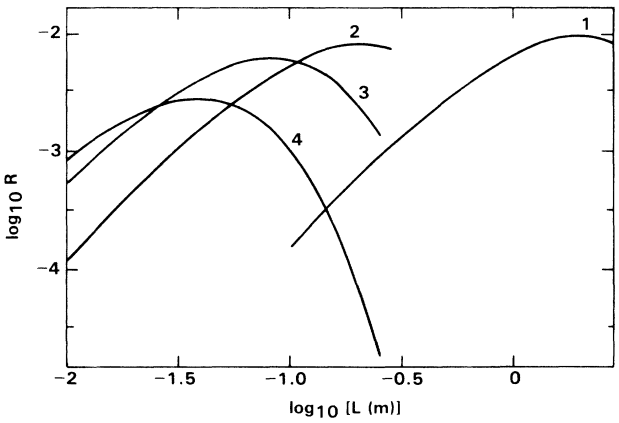

FIG. 6. Phase-conjugate reflectivity vs beam interaction length at $\lambda = 5145$ Å. Reduced temperatures are as follows: curve 1, $T_r = 10^{-2}$; curve 2, $T_r = 10^{-3}$; curve 3, $T_r = 10^{-3.5}$; curve 4, $T_r = 10^{-4}$. Pump intensities equal 10 kW/cm^2.

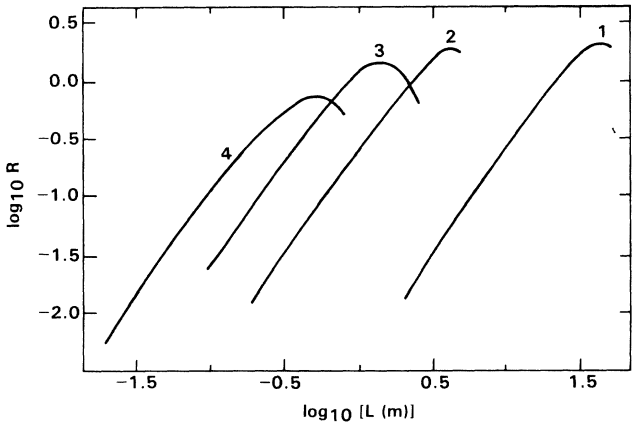

FIG. 7. Phase-conjugate reflectivity vs beam interaction length at $\lambda=1.06$ μm. Reduced temperatures are as follows: curve 1, $T_r=10^{-2}$; curve 2, $T_r=10^{-3}$; curve 3, $T_r=10^{-3.5}$; curve 4, $T_r=10^{-4}$. Pump intensities equal 10 kW/cm^2.

longer wavelength, oscillation is observed. Oscillation is seen in Fig. 8, which was derived for $\lambda=1.06$ μm, $T_r=10^{-3.5}$ and a cw pump intensity equal to 20 kW/cm^2. Other consequences of the foregoing theory are also apparent in these figures. For example, in Fig. 6, the curves labeled 1 and 2, for $T_r=10^{-2}$ and 10^{-3}, respectively, have nearly identical shape due to scaling. Referring to Fig. 3, this scaling behavior is seen to occur over the reduced temperature range for which the curves corresponding to σ_0 and κ_0 are linear and parallel. The same behavior occurs at $\lambda=1.06$ μm, as may be seen through a comparison of Figs. 4 and 7. Finally, the breakdown of scaling seen close to the critical temperature occurs as the correlation length approaches the natural length scale set by the grating spacing. This breakdown is yet another manifestation of the effect of long-range interactions included in the present calculations.

The final calculations presented in this section include the effect of noise. As noted previously, the full solution provided by Eqs. (4.13) and (4.14) for nonzero γ assumes that the phase and amplitude of this complex variable are fixed. However, from Eqs. (4.9) and (3.19) it is seen that

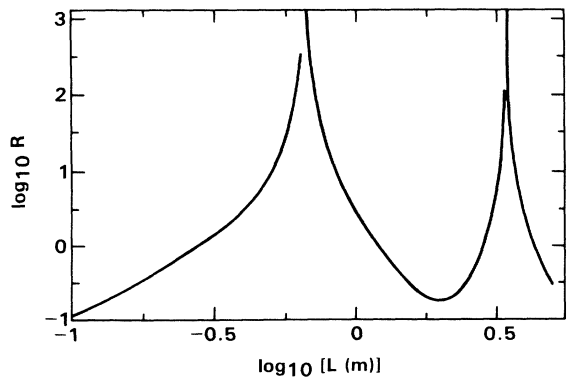

FIG. 8. Phase-conjugate reflectivity vs beam interaction length for $\lambda=1.06$ μm at $T_r=10^{-3.5}$. Pump intensities equal 20 kW/cm^2.

γ undergoes Gaussian fluctuations in time with

$$\langle|\gamma(\mathbf{q})|^2\rangle=(Q^2E_0^2/4\epsilon_0^2)\langle|\delta\epsilon(\mathbf{q})|^2\rangle$$
$$=(Q^2E_0^2/4\epsilon_0^2)8\pi kT\epsilon_2(\mathbf{q})/V_s \qquad (4.16)$$

and random phase. To make further progress, we observe that the fluctuations in γ vary on the time scale (τ) of the medium response, which is slow compared to the transit time of light through the medium. Accordingly, only the instantaneous value of γ is required to obtain a solution valid over a time interval that is short compared to the response time of the medium. This adiabatic approximation provides an especially convenient stochastic approach to calculating the effects of noise. Specifically, this approach consists of obtaining the solution to Eqs. (4.13) and (4.14) separately for each fixed-γ member of a statistical ensemble. The ensemble itself is defined to consist of the collection of solutions obtained for a representatively large number of values of γ. The present set of γ values, used in the calculations described below, was generated through computer sampling to have Gaussian statistics characterized by Eq. (4.16) [with ϵ_2 from Eq. (3.17)], and to satisfy the condition of random phase.

Results of stochastic noise simulation for the conjugate field are shown in Fig. 9. Without loss of generality, the incident probe field is taken to be real and is represented by the single point appearing on the real axis in Figs. 9(a)–9(d). A representative set of 101 values of γ was generated in the manner described above, and the corresponding number of solutions to Eqs. (4.13) and (4.14) for the conjugate field obtained. [Note that the coefficients c_1 and c_2 appearing in Eq. (4.13) must be recalculated for each solution.] The result is a cluster of points shown in the figure (one point for each solution) whose spread conveys both the amplitude and phase noise inherent in the conjugate wave. Each cluster is centered on the hypothetical noise-free (or zero-temperature) solution calculated for $\gamma=0$. The latter lies on the imaginary axis due to a phase shift of $\pi/2$ incurred in forming the conjugate wave. In addition to a dependence on the frequency of light and temperature, the noise power present in the conjugate wave was shown in Ref. 4 to depend only on the product $\kappa_0 L$ and on the *total power* in the entering probe beam. This same behavior is seen in Figs. 9 for the noise fluctuations in the field itself. Here each figure was obtained under conditions of the same temperature ($T_r=10^{-3.5}$) and wavelength ($\lambda=1.06$ μm) with $L=1$ m and pump intensity of 10 kW/cm^2. (These conditions lie near the maximum of curve 3 in Fig. 7 and near the threshold temperature for observable $\mathbf{q}$ dependence in Fig. 4.) Thus, the values of $\kappa_0 L$ and R are constant in Figs. 9(a)–9(d). Figures 9(a) and 9(b) were obtained for a total probe power of 1 W, but represent different probe intensities since the beam cross sectional areas differ by a factor of 1000 in the two figures. At 1-W probe power, the noise fluctuations are seen to be just barely resolvable on the scale of the figure. Figures 9(c) and 9(d) were each obtained for a total probe power of 1 mW and again represent different probe intensities. Here the noise fluctuations are much more pronounced and clearly show

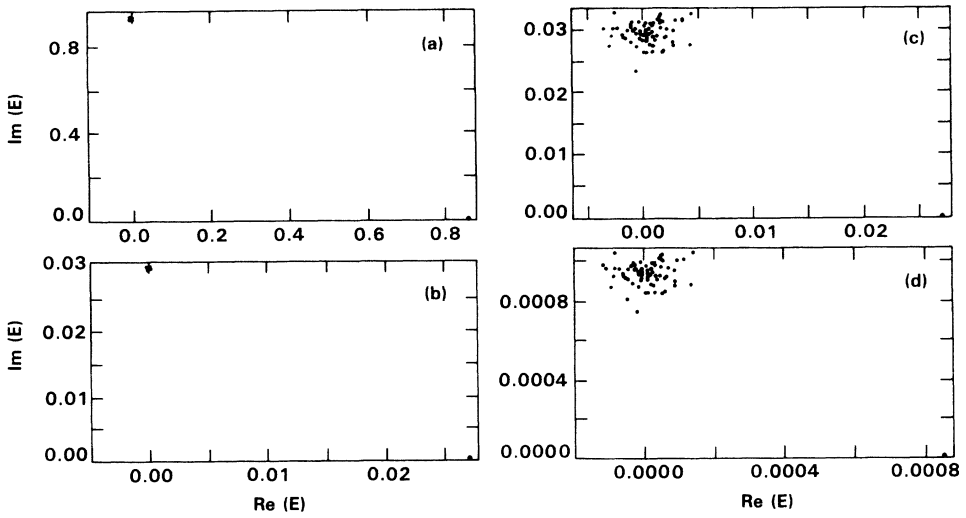

FIG. 9. Fluctuations in the real and imaginary components of the conjugate field due to light-scattering noise. Pump intensities equal 10 kW/cm^2, $\lambda=1.06$ μm, $T_r=10^{-3.5}$, and $L=1$ m. Results are for (a) probe power $=1$ W, probe beam area $=0.001$ cm^2; (b) probe power $=1$W, probe beam area $=1$ cm^2; (c) probe power $=0.001$ W, probe beam area $=0.001$ cm^2; (d) probe power $=0.001$ W, probe beam area $=1$ cm^2. Field strengths are in mks units.

that the relative range of scatter depends on the total power of the probe beam but not otherwise on its cross section area and intensity.

V. SUMMARY AND DISCUSSION

The fundamental connection between light scattering and nonlinear optical response has been developed for isotropic Kerr media and extended to include long-range correlations characteristic of fluids near a critical point. This extension has culminated in a fluctuation-dissipation relation [Eq. (3.19)] that provides a quantitative means for calculating nonlinear optical response directly from the known light-scattering properties of the medium. In addition, by incorporating light-scattering fluctuations directly into the equations governing beam propagation, the amplitude and phase noise characteristics of the medium were obtained.

In the preceding sections, the Ornstein-Zernike model for light-scattering fluctuations near a critical point was used in conjunction with the fluctuation-dissipation relation to derive the nonlinear optical response. Key findings are as follows: (1) The Kerr coefficient (ϵ_2 or n_2) acquires a wave-vector dependence that becomes more pronounced as the critical point is approached. Moreover, the form of this dependence is identical to that implied by the angular dissymmetry of light-scattering fluctuations in the Ornstein-Zernike model. (2) The size of the Kerr coefficient no longer diverges with the isothermal compressibility, but instead levels off, and in some cases is reduced (see Table I), as temperatures very close to the critical temperature are approached. (3) Identical wave vector and reduced temperature dependences for the Kerr coefficient and the structure factor are found. Similar properties [(1)–(3)] immediately follow for derived quantities such as the four-wave-mixing coefficient, shown here as a function of the reduced temperature in Figs. 3 and 4.

Preliminary experimental indications that simple critical-point fluids have exceptionally high potential for nonlinear optical signal processing applications[7] are supported by the results of the present study. For example, n_2 values of 10^{-15}–10^{-14} m^2/W and response times in the 1–10-μsec range are predicted here for xenon at the critical density and temperatures near T_c. Even when losses due to light scattering are properly taken into account, phase-conjugate reflectivity in excess of unity is predicted for 1.06-μm wavelength radiation and cw pump intensity in the 10-kW/cm^2 range. In addition, while our results show that light-scattering noise is significant at low signal powers, they also demonstrate that critical-point fluids are inherently no more noisy than other Kerr media when compared at the same temperature, optical frequency, and comparable values of $\kappa_0 L$.

Calculated values for the nonlinear index and response time for near-critical xenon, from Table I, are shown in Fig. 10 along with reported values for these quantities obtained for a selection of other Kerr and artificial Kerr media (see the caption). Entries 1, 2, 5, and 6 represent media with anisotropic molecules or particles capable of rotating into alignment with the applied field. The response times for these materials should be relatively insensitive to wavelength and grating spacing. Indeed, these entires are seen to span a wide range of wavelengths from the millimeter to the submicron (visible) regime. Entry 3 (present work) and entry 4, on the other hand, represent isotropic media whose response requires transport of molecules, density fluctuations, or particles over distances comparable to the grating spacing. For these cases the response times will depend on the grating spacing, as determined from the wavelength and angle of the writing beams. Both these entries are for $\lambda=5145$ Å, but for different grating spacings. Accordingly, the response time for entry 4 (which is proportional to q^{-2}) was de-

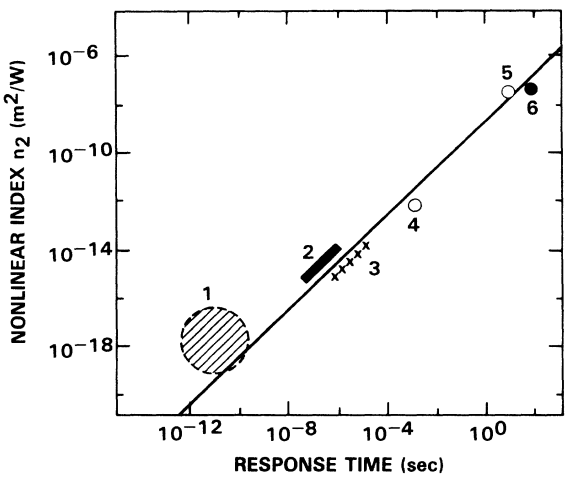

FIG. 10. Comparison with other Kerr media. Symbols represent (1) typical molecular Kerr liquids, e.g., CS_2, nitrobenzene; (2) isotropic phase liquid crystal near T^*, from Ref. 6; (3) xenon near T_c, present work; (4) aqueous polystyrene sphere suspension, from Ref. 1; (5) graphite rod suspension, based on millimeter wavelength birefringence measurements from Ref. 19; (6) nematic phase liquid crystal, from Ref. 20.

creased from its reported value in order to make the present comparison valid for the shorter (180° angle between writing beams) grating spacing. [A line of unit slope is included in the figure for comparison to show that the nonlinear index varies roughly inversely with the response time for the cases shown. More detailed examination of this dependence (which must be regarded as somewhat fortuitous for entries 3 and 4) is beyond the scope of the present study.] The comparison shows clearly that the predicted nonlinear optical properties of xenon are consistent with the measured properties reported for other types of nonresonant Kerr media. Specifically, the properties of critical-point fluids (entries 2 and 3) appear to lie intermediate between those of media that undergo fast molecular scale and slow large scale realignment in response to the electromagnetic field. For those applications requiring response times in the 1–100 μsec range, it is seen that critical-point fluids may have the largest Kerr-type nonlinear response.

ACKNOWLEDGMENTS

The author gratefully acknowledges Dr. Victor Wang, Dr. Glenn Bennett, and Dr. Kevin Schehrer of the Rocketdyne Division of Rockwell International for discussions of their experiments.

APPENDIX

Derivation of Eq. (2.11) using the OZ approach may be summarized as follows. First, the direct correlation function $C(\mathbf{R})$ is introduced through its Fourier transform

$$C(\mathbf{q})=\int C(\mathbf{R})\exp(i\mathbf{q}\cdot\mathbf{R})d^3\mathbf{R}$$

to have the property that

$$C(\mathbf{q})=\Gamma(\mathbf{q})/[1+\langle\rho\rangle\Gamma(\mathbf{q})]\ , \tag{A1}$$

where

$$\Gamma(\mathbf{q})=\int\Gamma(\mathbf{R})\exp(i\mathbf{q}\cdot\mathbf{R})d^3\mathbf{R}$$

is the Fourier transform of $\Gamma(\mathbf{R})$ defined in Eq. (2.5). Substitution of Eq. (2.4) into Eq. (2.3) gives

$$\begin{aligned}S(\mathbf{q})&=\langle\rho\rangle V_s[\langle\rho\rangle\Gamma(\mathbf{q})+1]\\&=\langle\rho\rangle V_s[1-\langle\rho\rangle C(\mathbf{q})]^{-1}\ ,\end{aligned} \tag{A2}$$

where to obtain the last equality, (A1) has been used. Now as T approaches infinity, $S(\mathbf{q})$ approaches $S^0(\mathbf{q})$ of Eq. (2.7), and $C(\mathbf{q})$ approaches zero. At critical point, $S(\mathbf{q})$ approaches infinity implying through (A2) that $C(\mathbf{q})$ approaches $1/\rho$. This behavior suggests that $C(\mathbf{R})$ remains short ranged even near the critical point and, therefore, provides support for the next step in the OZ approach; namely, the assumption that integrals of the form

$$\int R^k C(\mathbf{R})d^3\mathbf{R}\ ,$$

where $R=|\mathbf{R}|$ also remain finite. Expanding

$$\exp(i\mathbf{q}\cdot\mathbf{R})\approx 1+i\mathbf{q}\cdot\mathbf{R}-(\mathbf{q}\cdot\mathbf{R})^2\ ,$$

in the transform integral definition for $C(\mathbf{q})$, results in the following Taylor series about $q=0$:

$$C(\mathbf{q})=C_0-C_2q^2\ , \tag{A3}$$

where

$$C_0=4\pi\int R^2C(\mathbf{R})d^3\mathbf{R}$$

and

$$C_2=(2\pi/3)\int R^4C(\mathbf{r})d^3\mathbf{R}\ .$$

Terms involving higher powers of q are neglected. Now from Eqs. (2.7), (A2), and (A3),

$$S^0(\mathbf{q})/S(\mathbf{q})=1-\langle\rho\rangle C_0+\langle\rho\rangle C_2q^2\equiv R_0^2(q_0^2+q^2)\ , \tag{A4}$$

where

$$R_0^2=\langle\rho\rangle C_2$$

and

$$q_0^2=(1-\langle\rho\rangle C_0)/R_0^2\ .$$

From Eqs. (2.7)–(2.9) and (A4), we obtain

$$R_0^2q_0^2=(\langle\rho\rangle kT\beta_T)^{-1}\ .$$

Substitution of this last result into (A4) gives Eq. (2.11):

$$S(\mathbf{q})/S^0(\mathbf{q})=\langle\rho\rangle kT\beta_T[1+(q/q_0)^2]^{-1}\ . \tag{A5}$$

[1]P. W. Smith, P. J. Maloney, and A. Ashkin, Opt. Lett. **8**, 347 (1982).
[2]R. McGraw and D. Rogovin, SPIE **739**, 100 (1987).
[3]R. McGraw and D. Rogovin, in *Advances in Laser Science—III*, Proceedings of the Third International Conference, Atlantic City, New Jersey, 1987, AIP Conf. Proc. No. 172, edited by Andrew C. Tam, James L. Gole, and William C. Stwalley (AIP, New York, 1988), p. 253.
[4]R. McGraw, D. Rogovin, and A. Gavrielides, Appl. Phys. Lett. **54**, 199 (1989).
[5]R. Hellwarth, Phys. Rev. **130**, 1850 (1963).
[6]G. K. L. Wong and Y. R. Shen, Phys. Rev. A **10**, 1277 (1974).
[7]V. Wang, G. Bennett, P. Roullard, R. Hassler, and P. Stanley (unpublished).
[8]B. J. Berne and R. Pecora, *Dynamic Light Scattering* (Wiley, New York, 1976), Chap. 10.
[9]H. E. Stanley, *Introduction to Phase Transitions and Critical Phenomena* (Oxford, New York, 1971), Chap. 7.
[10]L. D. Landau and E. M. Lifshitz, *Electrodynamics of Continuous Media* (Pergamon, New York, 1960).
[11]R. D. Mountain, Rev. Mod. Phys. **38**, 205 (1966).
[12]M. Fixman, J. Chem. Phys. **33**, 1357 (1960).
[13]P. Debye, J. Chem. Phys. **31**, 680 (1959).
[14]H. Z. Cummins and H. L. Swinney, J. Chem. Phys. **45**, 4438 (1966).
[15]D. L. Henry, H. L. Swinney, and H. Z. Cummins, Phys. Rev. Lett. **25**, 1170 (1970).
[16]M. R. Moldover, Phys. Rev. A **31**, 1022 (1985).
[17]R. Hocken and M. R. Moldover, Phys. Rev. Lett. **37**, 29 (1976).
[18]D. M. Pepper and A. Yariv, in *Optical Phase Conjugation*, edited by R. A. Fisher (Academic, New York, 1983), Chap. 2.
[19]B. Bobbs, R. Shih, H. R. Fetterman, and W. W. Ho, Appl. Phys. Lett. **52**, 4 (1988).
[20]S. D. Durbin, S. M. Arakelian, and Y. R. Shen, Phys. Rev. Lett. **47**, 1411 (1981).